CONF-801011--41

ELECTROMAGNETIC EFFECTS INVOLVING A TOKAMAK REACTOR FIRST WALL AND BLANKET

by

L.R. Turner, K. Evans, Jr., D. Gelbard and R. Prater

Prepared for

Fourth American Nuclear Society Topical Meeting

on the

TECHNOLOGY OF CONTROLLED NUCLEAR FUSION

King of Prussia, Pennsylvania

October 14-17, 1980

ARGONNE NATIONAL LABORATORY, ARGONNE, ILLINOIS

Operated under Contract W-31-109-Eng-38 for the

U. S. DEPARTMENT OF ENERGY

ELECTROMAGNETIC EFFECTS INVOLVING A TOKAMAK REACTOR FIRST WALL AND BLANKET*

L. R. Turner, K. Evans, Jr., E. Gelbard and R. Prater**
Argonne National Laboratory
Argonne, Illinois 60439

Summary

Four electromagnetic effects experienced by the first wall and blanket of a tokamak reactor are considered. First, the first wall provides reduction of the growth rate of vertical axisymmetric instability and stabilization of low mode number interval kink modes. Second, if a rapid plasma disruption occurs, a current will be induced on the first wall, tending to maintain the field formerly produced by the plasma. Third, correction of plasma movement can begin on a time scale much faster than the L/R time of the first wall and blanket. Fourth, field changes, especially those from plasma disruption or from rapid discharge of a toroidal field coil, can cause substantial eddy current forces on elements of the first wall and blanket. These effects are considered specifically for the first wall and blanket of the STARFIRE commercial reactor design study.

Introduction

The first wall and blanket of a tokamak reactor are closely coupled magnetically with the plasma current and with the toroidal and poloidal magnet systems. Consequently they experience several electromagnetic effects. Four of these effects will be described here:

1. Plasma stabilization and reduction of plasma motion.
2. Protection of the reactor systems against the electromagnetic consequences of a plasma disruption.
3. Delay of the penetration of ohmic-heating flux and control field from coils outside the blanket into the plasma region.
4. Eddy current forces and torques on first wall and blanket components.

In general, the first two effects aid the operation of the reactor while the last two hinder it. However, it is difficult to take advantage of the former without having to deal with the latter.

* Work supported by the U.S. Department of Energy.
** General Atomic Company, San Diego, California.

First Wall and Blanket

The following discussions will make use of the concepts and parameters of the STARFIRE commercial reactor design study[1,2] in order to be specific.

Each STARFIRE blanket module[3] consists of a 1-cm thick first wall, a 7-cm thick neutron multiplier, a 40-cm thick breeding zone, and a 20-cm thick reflector that contains the blanket support structure and the manifolding. The modules are 2 to 3 m wide and approximately 3 m high depending on the location within the reactor. The module walls and all support structures in the high-radiation zone are fabricated from an advanced low-swelling austenitic stainless steel. All internal structure is integrally cooled to remove the nuclear heating and maintain the structure below 400°C. Figure 1 is a schematic drawing of a blanket module. Eight blanket modules arranged poloidally comprise a blanket sector, and twenty-four sectors arranged toroidally make up the complete blanket.

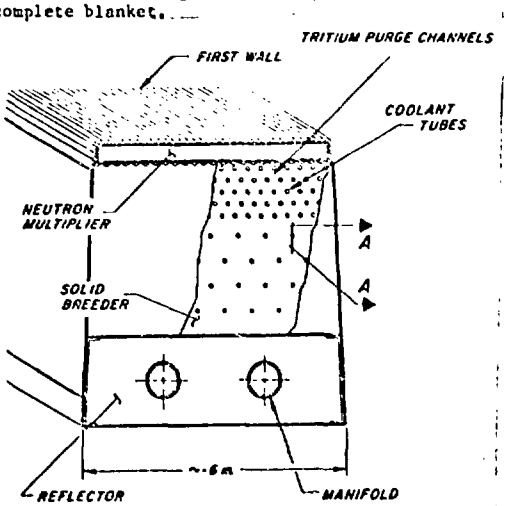

Fig. 1. Schematic drawing of a STARFIRE blanket module.

The austenitic stainless steel first wall is a panel coil-type construction and is an integral part of the blanket module. Panel coil-type construction provides integral cooling of the blanket wall and avoids the necessity for a large number of tube welds in the high radiation zone. A 1-mm thick beryllium coating or clad on the first wall serves to protect the plasma from the high-Z wall material.

The Zr_5Pb_3 neutron multiplier provides the design simplicity of a solid state material. A multiplier zone thickness of 7 cm is required for sufficient multiplication. The back side of the first wall and a water-cooled panel between the multiplier and breeder zones provides cooling for the 7-cm slab.

Within each module the first wall and neutron multiplier provide an electrical conductance equivalent to a 2 cm thick sheet of stainless steel. Electrical jumpers between modules complete conducting paths toroidally and poloidally.

L/R Time of the First Wall and Blanket

The electromagnetic effects are largely determined by τ, the L/R time of the first wall and blanket. Different L/R times might be expected for toroidal currents, which would result from a plasma disruption, and for poloidal currents, which would result from a fast toroidal field (TF) coil discharge. In either case, the current is assumed to be confined to the multiplier region, a 7 cm thick layer of Zr_5Pb_3.

For toroidal currents, the inductance is found from the expression for a hollow torus

$$L = \mu_o R\,[\ln(8R/a) - 2] = 9.0\ \mu H \qquad (1)$$

in which R = 7 m and a = 2.72 m, which gives an equivalent area. The resistance for an unbroken first wall is given by

$$R = 2\pi R\rho/p\delta \qquad (2)$$

where ρ is the resistivity of the multiplier material; δ its thickness and p = 18.6 m is the perimeter of the cross section. For Zr_5Pb_3, ρ/δ = 15.77 $\mu\Omega$ which yields R = 37.3 $\mu\Omega$. Consequently, the L/R time is τ = 240 ms. Finite resistance of the jumpers will lower that value. Earlier calculations including the resistance of the stainless steel blanket members to the jumper in the back yielded τ = 40 ms. In the following, τ = 40 ms and τ = 300 ms will both be considered.

For a poloidal current, the current is again assumed confined to the multiplier region. The inductance is found by considering the currents and flux which would follow an instantaneous TF coil discharge. The toroidal field B_{TF} is 5.8 T at the major radius of 7 m, and thus can be written as a function of radius r:

$$B_{TF} = 5.8\ T \times 7\ m/r = 40.6/r \qquad (3)$$

The flux ϕ is the integral of B_{TF} over a cross section bounded by the first wall

$$\phi = \int B_{TF}\,dA = 137.59\ Wb$$

The current I is given by $I = \oint J\delta d\ell$ where the integral is taken over the perimeter, and the current density J is given by $J\delta = B_{TF}/\mu_o$. Integration yields I = 85.6 MA. Thus $L = \phi/I = 1.607$ μH. The resistance R is approximately 40.6 $\mu\Omega$, and the L/R time, τ = 40 ms.

Plasma Stabilization and Reduction of Plasma Motion

Insofar as the first wall serves as a conducting shell, it provides reduction of the growth rate of the vertical axisymmetric instability and stabilization of the low mode number internal kink modes. The elongated STARFIRE equilibrium is unstable due to a negative index of curvature of the vertical field, and the uncorrected growth time for this instability is the poloidal Alfven time, which is of order 10 μs. Conducting segments of a close-fitting shell slow this time to the millisecond range, but maximum slowing occurs when the segments are interconnected in the toroidal direction.

The equation of motion of the plasma column for a vertical displacement may be given by

$$M\ddot{z} = 2\pi R_o I_p B_r\ , \qquad (4)$$

where B_r is the radial component of the magnetic field due to the equilibrium coils;

$$B_{vr} \approx -nzB_{vo}/R_o$$

is the radial field due to image currents flowing in an inductive first wall of minor radius r_u,

$$B_u \approx -\tau_u \dot{z}\mu_o I_o/2\pi r_u^2\ ,$$

where $\tau_u = 1/2\ \sigma\mu_o d_u r_u$ is the L/R time constant of the wall and d_u is the thickness of the wall, assumed small in comparison to the plasma minor radius. For the persisting mode, Eq. (4) reduces to

$$\dot{z} + z\frac{\gamma}{\tau_u} = \xi\frac{b_o}{\tau_u}\ , \qquad (5)$$

where

$$\gamma = -\frac{1}{2}\left(\frac{r_u}{R_o}\right)^2 n\Lambda_o,\quad \xi = \frac{r_u^2}{2R_o b_o}\Lambda_o\frac{B_d}{B_{vo}}\ ,$$

B_d is the radial component of a magnetic field disturbance, and b_o is the dimension of the plasma in the z-direction.

The solution to Eq. (5) is

$$\frac{z}{b_o} = \frac{\xi}{\gamma}\left(e^{\gamma t/\tau_u} - 1\right) \qquad (6)$$

for a step-function disturbance. The growth rate of the motion is

$$\tau = \frac{-2}{n\Lambda_0} \left(\frac{R_o}{r_u}\right)^2 \tau_u \ , \qquad (7)$$

which, for STARFIRE parameters ($n \approx -0.5$, $\Lambda_0 \approx 5$) is about four times the first wall time constant of 300 ms. Because the vertical displacement is unstable even if the initial disturbance is small, feedback control of every disturbance must be made on a time scale of about τ_u or shorter, in order to limit the displacement to a small fraction of the plasma minor radius.

Plasma analysis shows that low mode number kinks (n = 0,1,2,3) can be stabilized when the ratio of the shell minor radius to the plasma minor radius is less than about 1.1. In general, the image currents that flow in response to the plasma motions require a toroidally continuous conducting shell. When the toroidal continuity is made by intersegment jumpers, the stray inductance of the jumpers must be minimized in order to permit the image currents to follow the plasma motions.

The kink mode analysis is performed using the code ERATO.[4,5] The Lagrangian

$$L = \delta W_p + \delta W_v - \omega^2 \int \rho |\vec{\xi}|^2 d^3r$$

including plasma displacements $\vec{\xi}$ must be obtained to evaluate the MHD stability, where ω is the instability frequency, ρ is the plasma density, δW_p is the plasma potential energy, and δW_v is the vacuum potential energy. In the ERATO code, the displacement is expanded in toroidal eigenmodes $\xi = \xi_0 e^{-in\phi}$, where n is the eigenmode number and ϕ is the toroidal angle.

The calculation of the eigenvalue (kink mode growth rate) depends on the number of grid points used by the computer in calculating flux surface quantities and derivatives. The larger the number of grid points, the more accurate the result, but the more computer time required. The approach adopted here is to evaluate the eigenvalue for several values of N_ψ, the number of flux surfaces derived from the equilibrium calculations, and note the trend of the eigenvalue as N_ψ is increased and greater accuracy is achieved. Approximately, good convergence of the eigenvalue requires $N_\psi > 4nq_b$. For this reason, mode numbers higher than 3 or 4 are expensive to analyze due to the excessive number of grid points which must be used.

For the STARFIRE equilibrium, the growth rates of the n = 0,1,2 and 3 modes were examined. In this study, internal kink modes are considered under the assumption of a fixed plasma boundary shape. Stabilization of these modes may be achieved by use of a conducting wall surrounding the plasma. While some modes may be stable without the conducting wall in a circular equilibrium, low mode number kinks are unstable when the plasma cross-section is elongated.

Figure 2 shows the calculated growth rate for the n = 0,1,2,3 modes as a function of the inverse square of N_ψ (i.e., the inverse of the number of grid points). The safety factor on axis, q_a, is 1.27, which is above the minimum value required for interchange stability.

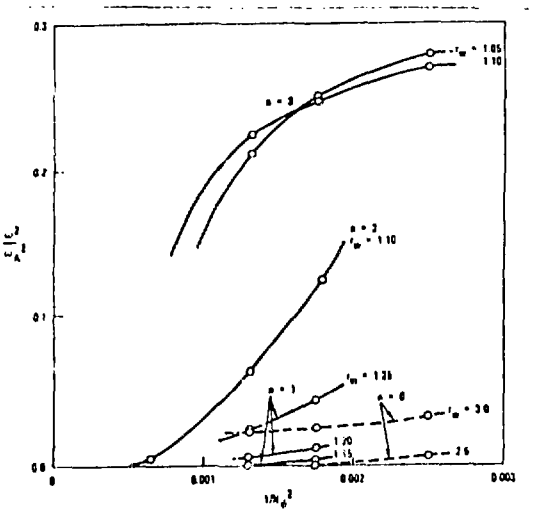

Fig. 2. Calculated growth rate for the n = 0,1,2,3 modes as a function of the inverse square of N_ψ.

The growth rate for each mode is plotted for several r_w, which is defined as the ratio of the distances from the plasma center to the conducting wall and to the plasma boundary. For the n = 0 mode, the square of the growth rate, γ^2, is about $0.1\ \omega_A^2$ when r_w is infinite, where ω_A is the Alfven frequency V_A/R, and V_A is the poloidal Alfven speed and R is the major radius.

The stabilizing effect of the conducting wall can be clearly seen, since for the n = 0 mode, γ^2/ω_A^2 drops to 0.02 for $r_w = 3.0$ and to 0 for for $r_w = 2.5$. As the mode number n increases, the instability becomes of smaller scale, so that the induced electrical currents in the wall must be closer to the plasma in order to effect stabilization. For the n = 1 mode, r_w must be less than about 1.15 for stabilization. For larger n, eigenvalue convergence becomes poorer, but the trend is toward stabilization for $r_w \sim 1.1$.

The pattern of local plasma displacements due to the unstabilized kink mode is that of small-scale vortexes in the direction across the flux surfaces. These displacements can cause rapid radial plasma transport. When the wall is moved close enough to the plasma

to cause stabilization of the kink mode, the displacement vectors become very small, and the displacements which remain tend to lie along the flux surface. These residual plasma motions cause little cross-field transport.

The most troublesome MHD instabilities may be the kink modes with toroidal mode numbers in the range of 4 to 10. These modes, and all higher modes, lie outside the range amenable to numerical analysis due to their small size relative to the numerical grid spacing. Kinks with large mode numbers may cause only moderately enhanced energy transport due to their fine scale, since the radial extent of the vortex is approximately proportional to $n^{-\frac{1}{2}}$, while the minor azimuthal angle of the vortex extent is proportional to n^{-1}. The intermediate modes may have sufficient extent to cause rapid transport, while not being amenable to wall stabilization owing to their small scale and distance from the wall. This difficulty with the kink modes is a characteristic of hollow current profiles in the STARFIRE case. If kink mode losses were too severe, the hollowness of the current density profile may need to be relaxed.

The conducting shell which surrounds the plasma and stabilizes the low mode number kinks must have toroidal continuity to be effective. In the STARFIRE design, these requirements are satisfied by conducting electrical jumpers between the toroidal spectors of the blanket.

Protection for Plasma Disruption

If a rapid plasma disruption occurs, a current will be induced on the first wall, tending to maintain the field formerly produced by the plasma. The field will then decay with the L/R time τ of the first wall and blanket rather than with shorter time constant τ_o of the plasma disruption.

The total plasma current is taken to be I_p = 10 MA. Calculations from plasma flux plots show that if the entire plasma current were instantaneously transferred to the first wall, the current per unit length around the perimeter would vary between 0.50 MA/m and 0.63 MA/m. This deviation from a uniform distribution should not be significant.

For the L/R time τ and an exponential plasma discharge with time constant τ_o, the first wall current is given by

$$I = \frac{I_p}{(1-\tau_o/\tau)} \left[e^{-t/\tau} - e^{-t/\tau_o}\right] \tag{8}$$

The maximum current occurs at time

$$t_{max} = \frac{-\tau_o \ln(\tau_o/\tau)}{(1-\tau_o/\tau)} \tag{9}$$

and is given by

$$I_{max} = \frac{I_p}{(1-\tau_o/\tau)} \left[\left(\frac{\tau_o}{\tau}\right)^{(\tau_o/\tau)(1-\tau_o/\tau)^{-1}} - \left(\frac{\tau_o}{\tau}\right)^{(1-\tau_o/\tau)^{-1}}\right] \tag{10}$$

Values of I_{max} and t_{max} are given in Table 1 for various values of τ_o for τ = 40 ms and 300 ms.

Table 1. Peak First Wall Current for Different Plasma Discharge Times

τ(ms)	τ_o(ms)	t_{max}(ms)	I_{max}(MA)
40	0	0	10.0
	10	18.5	6.30
	20	27.7	5.00
	50	44.6	3.28
	100	61.1	2.17
300	0	0	10.0
	100	165	5.77
	200	243	4.44
	400	345	3.16

The field external to the first wall will decay more slowly than it would without the conducting first wall; in general:

$$B(r,t) = B(r,0) \left[e^{-t/\tau} - (\tau_o/\tau)e^{-t/\tau_o}\right] / (1-\tau_o/\tau) \ . \tag{11}$$

Field Perturbation and Field Penetration Delay

In general, the inward penetration of an externally applied magnetic field occurs with the same L/R time which limits the outward penetration of flux resulting from plasma movement. However, position correction can begin in the much shorter time characterizing the distribution of current through the blanket thickness. This faster correction requires sensors within the blanket to detect the movement and requires correction coils outside the blanket which can respond with that shorter time.

Early tokamaks had conducting copper shells to keep the plasma in equilibrium. In most present day tokamaks the plasma is kept in equilibrium and centered in the chamber by an external coil system which is feedback-controlled. In these

experiments the thickness of the vacuum wall is kept small or else the wall has insulating breaks so that the variations in the external coil systems are transmitted to the plasma almost instantaneously.

A tokamak reactor, however, will have a thicker first wall, in which the radiation and heat make provision for dielectric breaks difficult. Poloidal field (PF) coils will be further away. The blanket and shield and possibly the TF coils lie between the plasma and the PF coils. It is necessary to determine the effects of these structures on the penetration of the external field.

There are two limiting cases to be considered. The first is a perfectly conducting wall, for which an external coil system would be superfluous. In the case of a plasma perturbation, the field lines in the chamber cannot move through the wall and their increased pressure as they are forced against the wall can provide a restoring force to the perturbation. Copper shell tokamaks depend on the fact that at least some modes are stabilized by such a wall. In the other case, representative of most present tokamak devices, the external field can control the plasma without hindrance. The reactor case with relatively thick, finitely conducting material falls between these two extremes: the external field has difficulty penetrating, but the fact that the internal field has trouble leaving may help make up for the slow penetration of the external field.

The model used is a cylindrical shell around a cylindrical plasma column (see Fig. 3). It is assumed there is no θ nor Z deperdence. The shell of outer radius, a, inner radius, b, thickness, $\Delta = a-b$, permeability, μ, and conductivity, σ, is fixed. The plasma radius, c, may vary. For the symmetry considered the radial component, B_r, of the magnetic field is zero, and the other components are determined by the equations:

$$\frac{1}{r}\frac{\partial}{\partial r}\left(r\frac{\partial B_z}{\partial r}\right) = \mu\sigma\frac{\partial B_z}{\partial t} \qquad (12)$$

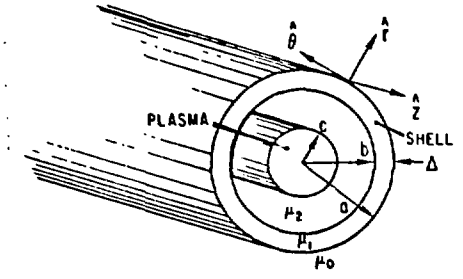

Fig. 3. Geometry of the plasma and shell model.

$$\frac{\partial}{\partial r}\frac{1}{r}\frac{\partial}{\partial r}(rB_\theta) = \mu\sigma\frac{\partial B}{\partial t} \qquad (13)$$

Two cases, which indicate the important mechanisms involved, are considered:

1. Diffusion of a longitudinal magnetic field through a shell surrounding a fixed radius, perfectly conducting plasma.
2. Diffusion of an azimuthal field needed to control a perturbed plasma whose radius varies.

Two time scales enter in both cases. The first $\tau = \mu\sigma\Delta^2$, is the time scale for diffusion through a material of thickness, Δ. The second is the L/R time, $\tau \approx \mu\sigma a\Delta$, of the shell. Since for a thin shell these time scales differ by a factor $\sim a$, it is important to determine which phenomena are associated with which time scale.

Diffusion of a Longitudinal Field

In this case the spatial and temporal dependence of B_z and E_θ are calculated subject to the boundary condition:

$$B_z(r = a,t) = B_o \qquad (14)$$

and the initial condition:

$$B_z(r,t = 0) = 0 . \qquad (15)$$

The plasma is assumed to be of fixed radius, c, and perfectly conducting.

It is first useful to calculate the form of the field in the vacuum region between the plasma and the shell. From the relationship, $\nabla \times \vec{B} = \mu\vec{J} = 0$, we get:

$$B_z = B(t) \qquad (16)$$

and from $\nabla \times \vec{E} = -\partial B/\partial t$, we get:

$$E_\theta = -\frac{r}{2}\frac{\partial \vec{B}(t)}{\partial t} + \frac{C(t)}{r} . \qquad (17)$$

The constant, C, is determined by the boundary condition $E_\theta(r = 0) = 0$, at the conducting boundary of the plasma:

$$C = \frac{c^2}{2}\frac{\partial B}{\partial t} . \qquad (18)$$

Since E_θ and B_z are continuous, the boundary condition at $r = b$ becomes:

$$\left.\frac{\partial B_z}{\partial r}\right|_b = \frac{\mu\sigma b}{2}\left[1 - \frac{c^2}{b^2}\right]\frac{\partial B_z}{\partial t} \qquad (19)$$

The boundary conditions (14) and (19) are sufficient to solve Eq. (12). The solution is shown in Fig. 4. It can be seen that the field diffuses into the shell without appreciably changing its value at $r = b$ on the time scale $\tau \approx \mu\sigma\Delta^2$.

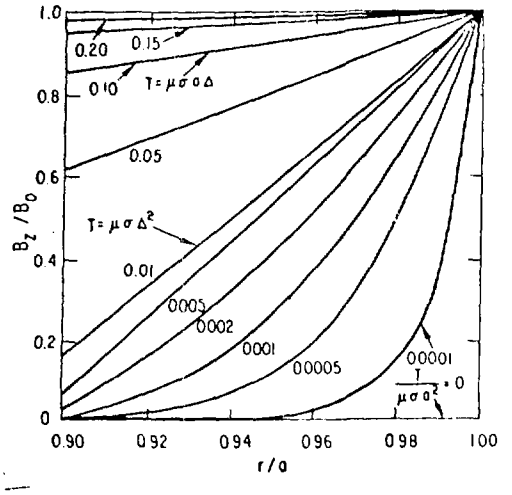

Fig. 4. The spatial and temporal dependence of $B_z(r,t)$ for the case $\Delta/a = 0.1$ and $c = 0$.

The change in $B_z(r = b)$, which involves a change in the poloidal current, can only occur on the longer L/R time scale. For the infinitely long shell the L/R time is $\tau = \frac{1}{2}\mu\sigma a\Delta$, and it can be noted that the field is $(1 - 1/e)$ of its final value at that time.

Diffusion of a Poloidal Correction Field

In order to determine how the control process works with a finite conducting shell around the plasma, it is necessary to have a model for the plasma motion. It is assumed that the plasma is perfectly conducting with a variable radius c. The plasma radius is determined by force balance:

$$p = \frac{B_\theta^2}{2\mu} \tag{20}$$

and the pressure is assumed to vary as:

$$p = \frac{k}{c^4} , \tag{21}$$

which can be shown to correspond to two dimensional adiabatic expansion. Initially the plasma is assumed to be in equilibrium with a poloidal field, $B_\theta(r = a) = B_0$, a radius, $c = c_0$, and a force constant, $k = k_0$.

At $t = 0$ the force constant is assumed to increase to $k = k_1$ as a result of an unspecified perturbation in the plasma dynamics. Because of the increase in pressure due to this perturbation, the plasma radius increases to $c = c_1$, where the preasure is again balanced by the magnetic preasure. The magnetic flux lines in the vacuum are compressed, but initially the field in the shell has not had time to change. The situation is shown schematically in Fig. 5.

At this time one can consider two options. The first is to leave the external field B_0 unchanged. This simulates passive control of the perturbation by the wall alone. The second is to notice that a perturbation has occurred and to change the external field to the field, B_1, necessary to bring the plasma back to its original radius. This simulates control of the plasma by an external field in the presence of the finitely conducting wall.

The radius c_1 is given by the expression:

$$k_o \log^2 \frac{b}{c_o} = k_1 \log^2 \frac{b}{c_1} . \tag{22}$$

If the external field is uncorrected, the plasma will eventually expand to a radius:

$$c_2 = c_o \left(\frac{k_1}{k_o}\right)^{\frac{1}{4}}. \tag{23}$$

The field needed to move the plasma back to radius c_o is given by

$$B_1 = \frac{c_2 B_0}{c_0} . \tag{24}$$

The problem is now to determine the spatial and temporal dependence of B_θ and E_z in each of the two cases:

$$B_\theta\ (r = a,t) = B_0 \text{ uncorrected} \tag{25}$$

$$B_\theta\ (r = a,t) = B_1 \text{ corrected} \tag{26}$$

Following the same procedure as before, we calculate the fields in the vacuum to be:

$$B_\theta = A(t)/r \tag{27}$$

$$E_z = \frac{\partial A(t)}{\partial t} \log \frac{r}{c} - \frac{A}{c}\frac{dc}{dt} \tag{28}$$

The force balance equation gives:

$$c = \left(\frac{2\mu k_1}{b\ B_\theta(b)}\right)^{\frac{1}{4}}, \tag{29}$$

and the boundary condition at $r = b$ becomes:

$$\frac{\partial}{\partial r}(rB_\theta)\Big|_b = \mu o b^2 \left[\frac{\partial B_\theta}{\partial t} \log \frac{b}{c} - \frac{B_\theta}{c}\frac{dc}{dt}\right]$$
$$= \mu o b^2 \left[\log \frac{b}{c} + 1\right] \frac{\partial B_\theta}{\partial t} \tag{30}$$

The boundary conditions (25 or (26) and (30) are sufficient to solve Eq. (13).

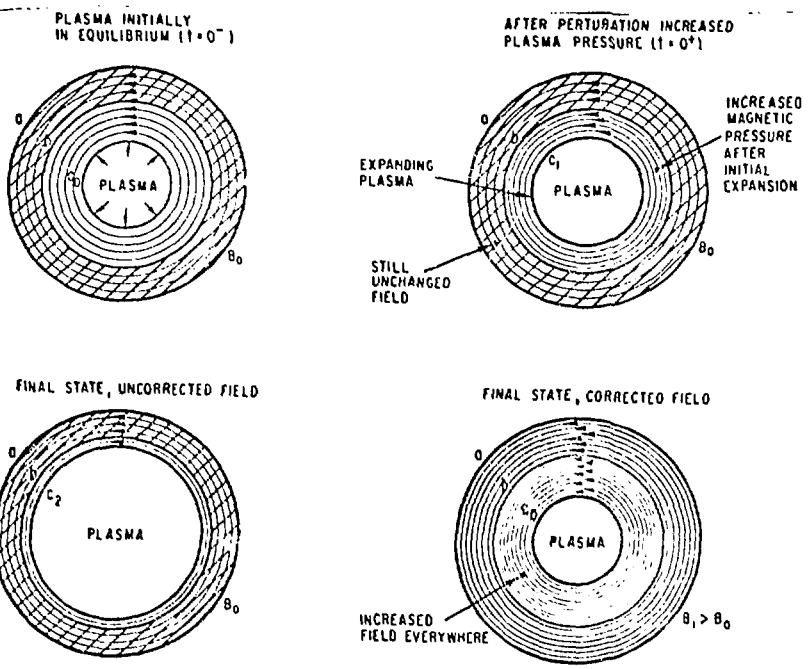

Fig. 5. Plasma and magnetic field behavior after a perturbation which increases the plasma pressure.

The motion of the plasma boundary for a typical case is shown in Fig. 6. It can be seen that the wall alone is only effective in controlling further expansion for a time much less than the L/R time. The wall alone never returns the plasma to its original position. On the other hand, the correction field is able to turn the plasma around on the short time scale, even through the plasma does not completely get back to its original position until after L/R time. It seems apparent that substantial control on time scales as fast as $\tau \approx \mu\sigma\Delta^2$ is possible with an intervening conducting structure between the plasma and the control coils.

Eigenvalue Interpretation of Results

An understanding of the above results involving the two time constant $\tau_1 \sim \mu\sigma a\Delta$ and $\tau_2 \sim \mu\sigma\Delta^2$ can perhaps be gained by considering a normal mode analysis of the problem. As in Fig. 3, we consider a long conducting hollow cylinder of inner radius b, outer radius a, wall thickness $\Delta = a-b$, and conductivity σ. For simplicity, we set the plasma radius c equal to zero. Fields

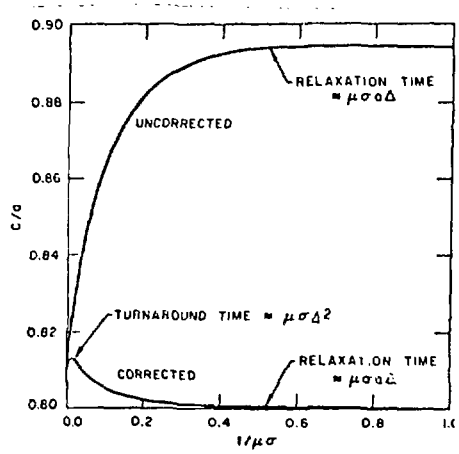

Fig. 6. Time dependence of the plasma radius following a plasma perturbation for the case $c_0/a = 0.80$, $C_1/a = 0.81$, and $\Delta/a = 0.1$. The behaviors when the motion is corrected or uncorrected are shown.

parallel to the axis of the cylinder and fields perpendicular to it give the same results, both are discussed here.

For the field parallel to the axis, each normal mode obeys

$$\nabla^2 B_Z = \sigma\mu \frac{\partial B_Z}{\partial t} = \frac{-\sigma\mu}{\tau} B_Z \qquad (31)$$

for $B_Z \sim e^{(-t/\tau)}$. As there is no Z or θ dependence,

$$\frac{1}{r}\frac{d}{dr}\left(r\frac{dB_Z}{dr}\right) = \frac{-\sigma\mu}{\tau} B_Z \, . \qquad (32)$$

Equation (32) has the asymptotic solution (which is adequate in the case $\Delta \ll b$)

$$B_Z = \sin(kr-\phi)/\sqrt{r} \qquad (33)$$

with k and φ to be determined by the boundary conditions:

$$B_Z = 0 \text{ at } r = a \qquad (34)$$

$$\frac{dB_Z}{dr} = \frac{\mu\sigma b}{2}\frac{dB_Z}{dt} = \frac{-\mu\sigma b}{2\tau} B_Z \text{ at } r = b. \qquad (35)$$

Equation (34) implies $\phi = ka$ and Eq. (35) implies

$$\tan[k_n b(\Delta/b)] = 2\, k_n b/[(k_n b)^2-1]. \qquad (36)$$

For small values of Δ/b, the first value of

$$\tau_n = \sigma\mu/k_n^2 \qquad (37)$$

is

$$\tau_1 = \sigma\mu b\Delta/2 \, . \qquad (38)$$

For $n \geq 2$, the right hand side of Eq. (36) is small; consequently

$$k_n b(\Delta/b) = k_n \Delta \approx (n-1)\pi$$

and

$$\tau_n = \sigma\mu\Delta^2/(n-1)^2\pi^2, \; n > 1 \, . \qquad (39)$$

For the field perpendicular to the axis, it is convenient to work with the vector potential $\bar{A}$.

$$\begin{aligned} \bar{A} &= \bar{k}A_Z(r)\sin\theta \exp(-\lambda t) \\ \bar{E} &= \frac{\partial \bar{A}}{\partial t} = \lambda\bar{A} \\ \bar{B} &= \nabla\times\bar{A} \\ B_r &= \frac{1}{r}\frac{\partial A}{\partial \theta} = \frac{1}{r}A_Z(r)\cos\theta \exp(-\lambda t) \\ B_\theta &= \frac{-\partial A}{\partial r} = \frac{dA_Z}{dr}\sin\theta \exp(-\lambda t) \end{aligned} \qquad (40)$$

For $r < b$, $A_Z \sim r$, and

$$A = B_0 r \sin\theta \exp(-\lambda t). \qquad (41)$$

Within the conductor, $b < r < a$, A_Z is given by the the asymptotic solution to Bessel's differential equation

$$A = C\, r^{-\frac{1}{2}}\sin(kr-\phi)\sin\theta \exp(-\lambda t) \, . \qquad (42)$$

Outside the cylinder, for

$$r < a, \; A_Z \sim 1/r, \text{ and } A = D \sin\theta \exp(-\lambda t)/r \qquad (43)$$

where C and D are constants to be determined from the boundary conditions. At $r = b$, E and B_θ are continuous; thus

$$\tan(k_n b-\phi) = k_n b/2 \, . \qquad (44)$$

At $r = a$, E and B_θ are again continuous; thus,

$$\cos(k_n a-\phi) = 0 \text{ or } \phi = ka-\pi/2 \qquad (45)$$

Equations (44) and (45) combine to give

$$\tan\left[k_n b(\Delta/b)\right] = 2/k_n b \, . \qquad (46)$$

Note that Eqs. (36) and (46) differ only by terms of order $(kb)^{-2}$, which are negligible where the asymptotic solution of Bessel's equation, Eq. (33), is valid. Thus, for the case of a field perpendicular to the axis also, the characteristic times are given by Eqs. (38) and (39).

In other words, the two times which enter the analysis above are the characteristic times corresponding to the first two normal modes of the geometry.

Eddy Current Forces and Torques

Eddy current forces due to TF coil discharge and to plasma disruption are described below. Forces due to charging the TF coils or equilibrium field (EF) coils or to a normal or abnormal EF coil discharge are much smaller than those described for the TF coil discharge and plasma disruption.

Forces from Discharge of TF Coil System

When the TF coils discharge, poloidal eddy currents are induced in the blanket with an L/R time of $\tau = 40$ ms, as shown above. This is much shorter than the TF coil discharge time τ_0; the shortest possible value for τ_0 is judged to be more than four seconds, a hundred times as long. The design value for τ_0 in case of a TF coil quench is 135 s.

Because the eddy currents are poloidal and because the toroidal field is much larger than the poloidal, the major force effect is a magnetic

pressure difference across the first wall, tending to explode the first wall. The pressure F/A is given by

$$F/A = J\delta B \qquad (47)$$

where J is the current density, δ is the wall thickness, and B is the magnetic field. Since $\tau \ll \tau_0$, the induced field can be ignored, and B can be taken to be the toroidal field.

On the inboard side of the first wall, r = 4.9 m, the toroidal field is largest, B = 8.27 T. For an instantaneous discharge, J = B/μ_0 = 6.58 MA/m, and F/A = 54.4 MN/m^2. For L/R time τ and TF coil decay time τ_0,

$$F/A = 8.27 \exp(-t/\tau_0)\ 6.58\ [\exp(-t/\tau) - \exp(-t/\tau_0)]/(1-\tau_0/\tau)$$

or

$$F/A = 54.4\ \mathrm{MN/m^2}\ [\exp\{-t(1/\tau + 1/\tau_0)\} - \exp(-2t/\tau_0)]/(1-\tau_0/\tau) \qquad (48)$$

which takes on its maximum value at

$$t_{max} = -\tau_0 \ln[(1 + \tau_0/\tau)/2]/(1-\tau_0/\tau) \qquad (49)$$

Table 2 gives t_{max} and F/A_{max} for τ = 40 ms and various values of τ_0. Note that even for discharge as fast as 4 s, the pressures are not unmanageable.

Table 2. Maximum Force on First Wall Due to TF Coil Discharge for τ = 40 ms

τ_0	t_{max}(s)	F/A (MN/m^2)	FA/(psi)
0	0	54.4	7880
1	0.107	1.69	245
4	0.158	0.50	72
40	0.249	0.054	7.8
135	0.297	0.016	2.3

Forces from Plasma Disruption

As described above, a plasma disruption will induce a toroidal current in the first wall. Being strictly toroidal, the current does not interact with the toroidal field. (In an earlier blanket design, the conducting jumpers between sectors were located at the back of the blanket modules, and the radial currents on the two sides of each module produced a large torsional stress on each blanket sector. With the jumper at the first-wall side, that stress does not occur.)

The eddy current interacts with its own field and with the decaying field from the plasma to given an average magnetic pressure F/A

$$F/A = IB\Delta\ell/p\Delta\ell = IB/p \qquad (50)$$

where I is the total induced current, B is the net toroidal field, and p is the perimeter. All the current interacts with the plasma field, B_p, but only half with the self field, B_s, since the self field varies from zero to its peak value across the current thickness,

$$F/A = (B_p + \tfrac{1}{2} B_s)\ I/p$$

Now $B_p = B_o \exp(-t/\tau_o)$

but B_s is proportional to the current, given by Eq. (8)

$$B_s = B_o\ (1-\tau_o/\tau)^{-1}\ [\exp(-t/\tau) - \exp(-t/\tau_o)]$$

The field at the first wall due to the full plasma, B_o is nearly equal to 1.0 T, and is related to the variables in Eq. (50) by

$$B_o = \mu_o I_p/p$$

Hence,

$$F/A = \frac{B_o^2}{2\mu_o(1-\tau_o/\tau)^2}\ [e^{-t/\tau} - (1-2\tau_o/\tau) \cdot e^{-2t/\tau_o} - 2\tau_o/\tau\ e^{-t(1/\tau + 1/\tau_o)}], \qquad (51)$$

and $B_o^2/2\mu_o$ = 0.398 MN/m^2 = 57.7 psi.

The maximum pressure, F/A_{max}, and the time at which it occurs, t_{max}, must be found by trial and error from Eq. (51). The maxima for τ = 40 ms and τ = 300 ms are shown in Table 3 for various values of τ_o. Because the expected values of τ_o do not greatly exceed τ, the peak pressure is not strongly dependent on τ_o.

Table 3. Maximum Magnetic Pressure on First Wall for Different L/R Times and Plasma Discharge Times

τ (ms)	τ_o (ms)	t_{max} (ms)	F/A_{max} (MN/m^2)	F/A_{max} (psi)
40	0	0	0.398	57.7
	1	2	0.369	53.4
	10	10	0.280	40.6
	20	16	0.235	34.1
	50	28	0.171	24.8
	100	41	0.124	18.0
300	0	0	0.398	57.7
	100	95	0.262	38.0
	200	145	0.216	31.4
	400	220	0.166	24.1

References

1. C. C. Baker, et al., "STARFIRE - A Commercial Tokamak Fusion Power Plant Study," Argonne National Laboratory, ANL/FPP-80-1 (1980).

2. C. C. Baker, et al., "An Overview of the STARFIRE Reference Commercial Fusion Power Reactor Design," Fourth ANS Topical Meeting on the Technology of Controlled Nuclear Fusion, King of Prussia, Pennsylvania (October 14-17, 1980).

3. D. L. Smith, et al., "First-Wall/Blanket Materials Selection for STARFIRE Tokamak Reactor," Fourth ANS Topical Meeting on the Technology of Controlled Nuclear Fusion, King of Prussia, Pennsylvania (October 14-17, 1980).

4. L. C. Bernard, et al., "Stabilization of Ideal MHD Modes," General Atomic Company, GA-A15236 (1979).

5. D. Berger, et al., Proc. Plasma Physics and Controlled Nuclear Fusion Research, IAEA Vienna, Vol. 2, 411 (1976).

6. L. R. Turner, "Safety of Superconducting Magnets for Fusion: Thermal and Electromagnetic Effects of Rapid TF Coil Discharge," Fourth ANS Topical Meeting on the Technology of Controlled Nuclear Fusion, King of Prussia, Pennsylvania (October 14-17, 1980).